LA-UR- 99-631

Approved for public release; distribution is unlimited.

Title: Directed Light Fabrication of Refractory Metals and Alloys

Author(s): Joe C. Fonseca, MST-6
Gary K. Lewis, MST-6
Patrick G. Dickerson, MST-6
Ron B. Nemec, MST-6

Submitted to: Report of Work Complete Under Order No. FA0000020AN
Contract DE-AC-12-76SN00052

Los Alamos
NATIONAL LABORATORY

DISCLAIMER

Directed Light Fabrication of Refractory Metals and Alloys

Joe C. Fonseca
Gary K. Lewis
Patrick G. Dickerson
Ron B. Nemec

Group MST-6
Materials Science and Technology Division
Los Alamos National Laboratory
Los Alamos, New Mexico, 87545

Abstract

This report covers work performed under Order No. FA0000020 AN Contract DE-AC12-76SN00052 for deposition of refractory pure metals and alloys using the Directed Light Fabrication (DLF) process and represents our progress in depositing these materials through September 1998.

In extending the DLF process technology to refractory metals for producing fully dense, structurally sound deposits, several problems have become evident. 1. Control of porosity in DLF-deposited refractory metal is difficult because of gases, apparently present in commercially purchased refractory metal powder starting materials. 2. The radiant heat from the molten pool during deposition melts the DLF powder feed nozzle. 3. The high reflectivity of molten refractory metals, at the Nd-YAG laser wavelength (1.06μm), produces damaging back reflections to the optical train and fiber optic delivery system that can terminate DLF processing. 4. The current limits on the maximum available laser power to prevent back reflection damage limit the parameter range available for densification of refractory metals.

The work to date concentrated on niobium, W-25Re, and spherodized tungsten. Niobium samples, made from hydride-dehydride powder, had minimal gas porosity and the deposition parameters were optimized; however, test plates were not made at this time. W-25Re samples, containing sodium and potassium from a precipitation process, were made and porosity was a problem for all samples although minimized with some process parameters. Deposits made from potassium reduced tungsten that was plasma spherodized were made with minimized porosity. Results of this work indicate that further gas analysis of starting powders and de-gassing of starting powders and/or gas removal during deposition of refractory metals is required.

Introduction

Using the Directed Light Fabrication (DLF) process, components are created from a three-dimensional computer aided design (CAD) representation. Through a computer aided manufacturing (CAM) package, motion paths are produced that drive the DLF equipment to trace all volumes of the desired component with the focal zone of a laser beam. Metal powders are introduced into the focal zone of the laser beam where they melt and re-solidify to form the part[1]. The DLF process has shown the ability to process hard to fabricate materials, such as Inconel 690[2], along with common materials like 316 stainless steel[3].

Figure 1 schematically shows the DLF process for single-pass (thin) and multi-pass (thick) plate deposition. A single-pass plate is built with a single laser pass and is as thick as the diameter of the molten pool after it solidifies. Each layer is made by traversing the molten pool created by the melting of incoming powder and substrate across the width of the plate. Multi-pass plates are built up to any thickness by overlapping laser passes as shown in the right diagram in Figure 1. The laser beam is incrementally moved vertically, creating the layer depth. Layers are added to produce the desired height and width of the plate. The variables for processing are the laser power, traverse speed, powder feed rate, horizontal overlap and vertical increment. These are all adjusted to achieve full density deposits.

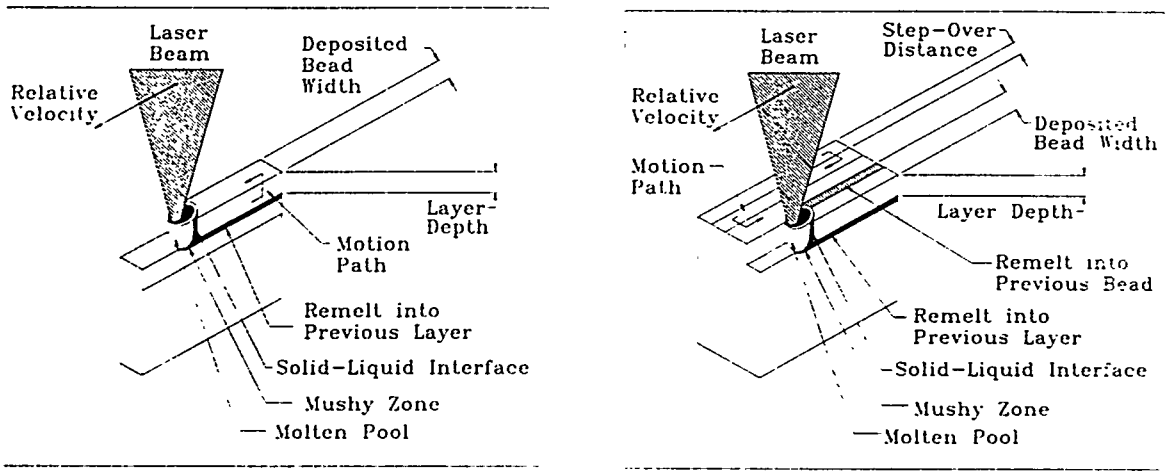

Figure 1. DLF deposition of a single-pass (thin) plate is shown on the left, which has a thickness equal to the molten pool diameter. Any thickness of plate can be built up by overlapping passes as shown for the plate on the right. Processing is performed in an argon atmosphere at oxygen impurity levels of 1-20ppm.

Creating three-dimensional components out of refractory metals and alloys is difficult and expensive using conventional processing methods. High melting temperatures, difficulty in working, and difficulty in machining make

powder metallurgy and EDM machining processes necessary. Therefore, it is a logical extension to use DLF to densify refractory metals in a single step to reduce processing times and cost.

KAPL Program

Work was initiated by Knolls Atomic Power Laboratory (KAPL) to create two rectangular plates for each refractory metal supplied, that were 0.280-in-thick by 1.750-in-tall by 1.90-in-long. Seven compositions of pure and blended powders were supplied. The work plan was to develop the necessary DLF process parameters to produce full density parts and then produce plates of the specified size for mechanical testing at Knolls Atomic Power Laboratory.

Powder Morphology

Starting powder morphologies are shown in Figures 2-4 for the powders studied. W-25Re, Figure 2 and Nb, Figure 3, are compared to plasma spherodized tungsten, Figure 4. The W-25Re was assumed to be produced by mixing tungsten and rhenium powders created by a potassium or sodium reduction process. The niobium was assumed to be produced by

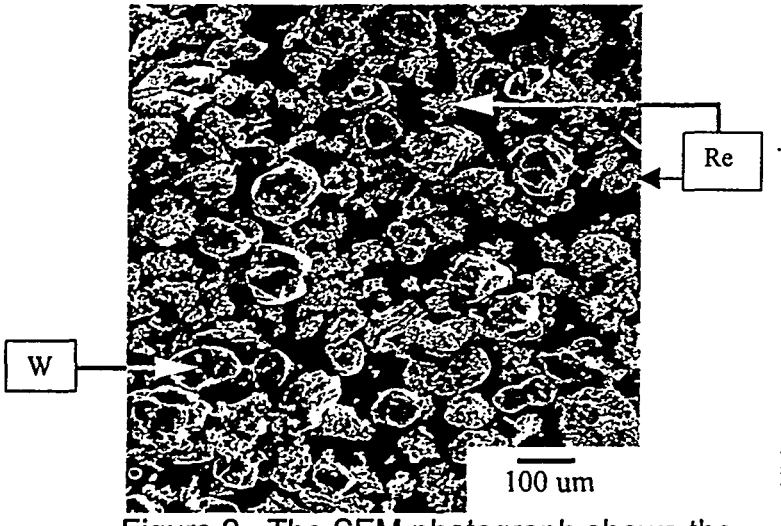

Figure 2. The SEM photograph shows the W-25Re blended powder particles, assumed to be Na or K reduced precipitate. EDS confirmed that the agglomerations were Rhenium particles.

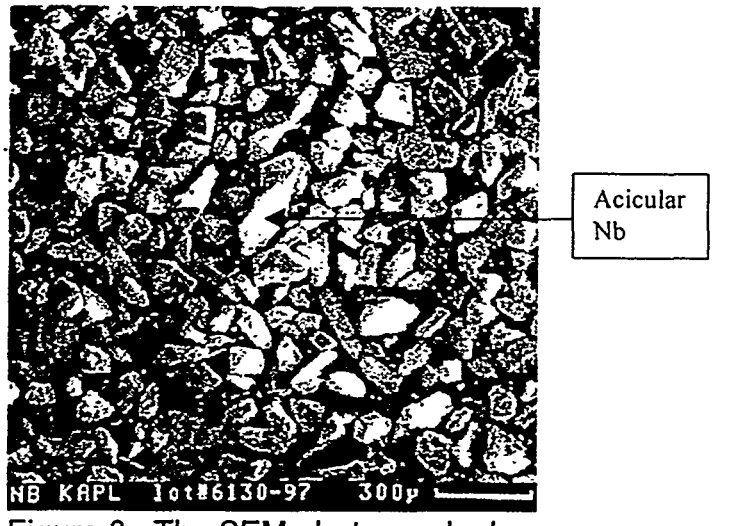

Figure 3. The SEM photograph shows niobium powder particles, (-200mesh), assumed to be made by electron beam melting, hydride de-hydride processing. Acicular shaped particles produced some nozzle clogging during DLF processing.

electron-beam melting followed by hydriding, crushing and de-hydriding. The spherical tungsten powder was potassium reduced and then plasma arc atomized to produce spherical powder. Although the tungsten was not included in the KAPL matrix of desired alloys, densification studies were performed and

reported here because the as-deposited porosity was minimized relative to our experience with sodium and potassium reduced powders.

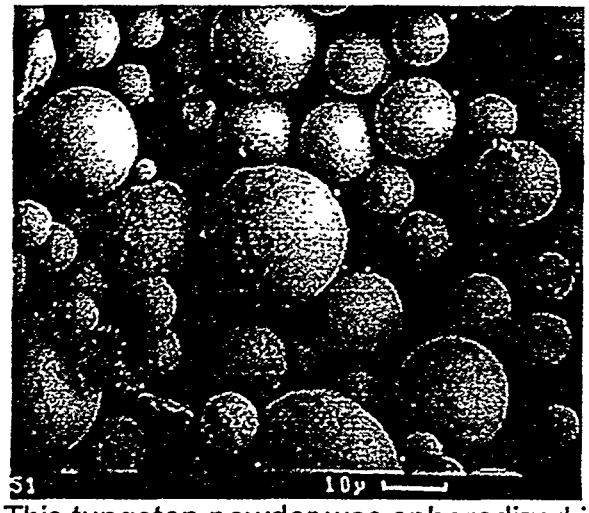

Figure 4. This tungsten powder was spherodized in a plasma arc to reduce gas content from the potassium reduction process.

In previous work, DLF had been used for deposits of tungsten, rhenium, tantalum and iridium. All of these materials with the exception of the plasma spherodized tungsten had unacceptable levels of porosity after deposition by the DLF process. In comparison the tungsten spherodized powder could be processed with minimal or zero porosity using DLF, as shown in Figure 5.

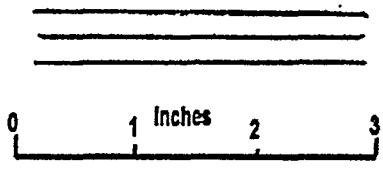

0.25-in-dia at 0.14 in/min.

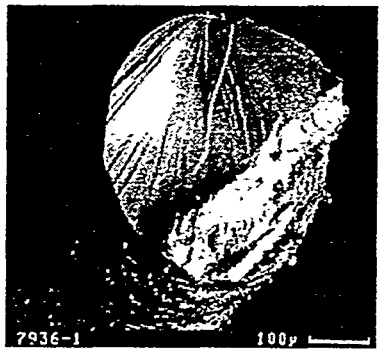

DLF Tungsten Fracture surface

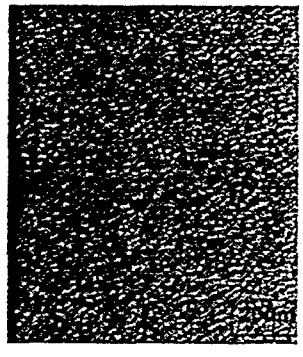

DLF Rod-Etched

Figure 5. Fully dense tungsten rods deposited by DLF are shown (left) with fracture surface (center) and microstructure (right). Spherodized powder was used and no voids (gas porosity) were observed.

Tungsten wires were formed with no evidence of porosity in the microstructure, however plate structures were not made. Rod cooling rates have been

measured to be 100 times lower than for plates, which might imply a longer dwell time for gas evolution from the molten pool during solidification.

Gas Dissolution in Powders

In previous work, interstitial gas contents measured on tantalum powder and tantalum DLF deposits, Table 1, showed the gas concentration actually decreased after DLF processing because the process melts and re-solidifies the material. However, porosity was still evident as spherical bubbles formed in the microstructure of these tantalum deposits, Figure 6.

Table 1. Interstitial content in Cabot tantalum and DLF deposit (ppm)				
	C	O	N	H
Cabot Ta Powder	72	726	30	21
DLF Ta Deposit	79	646	17	13

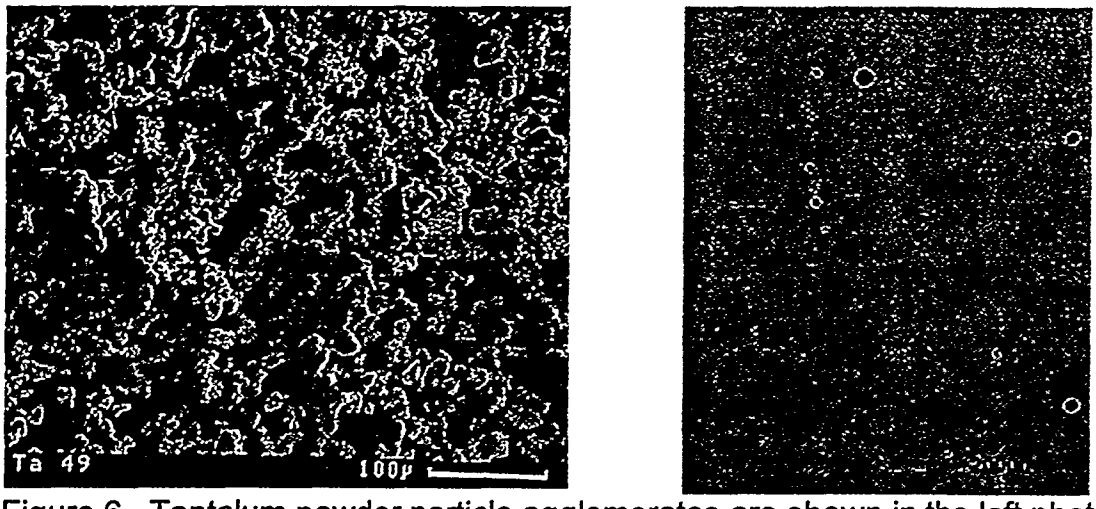

Figure 6. Tantalum powder particle agglomerates are shown in the left photo and the Ta DLF Deposit microstructure showing bubble formation is shown on the right. Note the similarity in agglomerates to Re (Figure 2).

From this prior history, we concluded that gases in the starting powders is the primary cause of porosity in the DLF deposits. Solubility of gases in metals is generally much higher in the liquid than in the solid at the melting point. Consequently as the liquid freezes, rejection of the gas at the solid-liquid interface could produce gas concentrations in the remaining liquid that exceed the solubility of the gas in the liquid, producing bubbles. This porosity was observed in all sodium and potassium reduced powders; however, powder re-melting, in the case of tungsten powder, produced minimal to zero porosity as observed in the microstructure. We have not performed sodium and potassium gas analysis on powders and deposits to see if these elements create the gas at the high melting points of refractory metals. An approach to further define and improve the DLF processing of refractory metals was developed for this program.

It was decided to both explore the DLF process parameter range to determine if porosity could be minimized and to look further at the starting powder chemistry and its production method. Materials were supplied and chemical analysis was provided by the vendors as shown in Table 2. Further chemical analysis was done at Los Alamos to measure gas content of the as-received powders, Table 3. In both the W-25Re and previous Ta work, a larger amount of porosity was observed, compared to the plasma spherodized W. Suspect elements that could

Table 2. Plate Compositions and Chemistry

Plate Materials		Powder Chemistry of Supplied Powders (vendor Analysis) in ppm.													
		Ta	Nb	Mo	W	Hf	Zr	Ti	Na	K	Ca	H	O	N	C
1. Ta		Bal.	25	10	25	-	-	5	13	46	2	46	488	11	10
2. Nb		1300	Bal.	<10	<10	<10	86	-	-	-	-	19.7	1400	67	44
3. Nb -1% Zr	Nb	1300	Bal.	<10	<10	<10	86	-	-	-	-	19.7	1400	67	44
	Zr	NL	NL	NL	NL	20000	Bal.	3000	NL	NL	1500	NL	NL	NL	-
4. W -25% Re	W	-	-	<300	Bal.	-	-	-	-	<10	-	-	-	-	<20
	Re	-	-	25	-	-	1	2	-	11	2	5	40	10	10
5. Mo - 50% Re	Mo	-	-	Bal.	-	-	-	<10	-	-	<10	-	-	-	10
	Re	-	-	25	-	-	1	2	-	11	1	5	40	10	20
6. Ta - 10% W	Ta	Bal.	25	10	25	-	-	5	13	46	2	46	488	11	10
	W	-	-	<300	Bal.	-	-	-	-	<10	-	-	-	-	<20
7. Nb - 10% Hf - 1% Ti	Nb	1300	Bal.	<10	<10	<10	86	-	-	-	-	19.7	1400	67	44
	Hf	NL	NL	NL	NL	Bal.	30000	NL	NL	NL	-	NL	NL	NL	-
	Ti	-	-	-	-	-	-	Bal.	-	-	-	360	2400	100	230
8. Plasma Spherodized W		-	-	8	Bal.	-	-	-	-	-	1	-	110	11	10

Bal. indicates the sample's balance of material. NL stands for not listed on spectrographic analysis sheets. - indicates no reading during spectrographic analysis. Rhenium did not occur as a residual in any of the other elemental blends from the given analysis, so it was omitted from the chart.

Table 3. Interstitial Analysis on Powdered Metals

Material	Chemical analysis (in ppm)			
	H	C	N	O
1. Plasma Spherodized W (LANL)	<1	47.9	35.7	309.0
2. Nb (KAPL)	41.9	103.5	70.6	1308.0
3. W-25% Re (KAPL)	1.4	60.1	40.3	495.6
4. W (LANL)	<1	14.5	33.3	148.6
5. Ta (LANL)	2.4	32.4	25.5	405.3

Chemical analysis done on powders provided by KAPL and internal stock. Analysis was done at Los Alamos National Laboratory.

cause gas porosity during solidification are O, N, H, C, Na, and K present in the starting materials and argon present in the processing box. For Nb, hydride de-

hydride powder, oxygen contents were 1400ppm and 1308ppm from the two analyses. For blended W-25Re, Na/K reduced powder, oxygen levels were at 495.6ppm and 40 for the LANL and vendor analyses, indicating a discrepancy. Oxygen levels are suspect for many of the materials and is the most abundant gas present. Measurement of gas concentration in DLF deposited plates was not performed.

Deposition Results

DLF deposition samples were made of W-25Re and pure Nb, supplied by KAPL, and plasma spherodized tungsten supplied by LANL. Plates, 0.280-in in thickness for the W-25Re and Nb, were deposited for microstructural evaluation to optimize process parameters. Single-pass plates, as described above, were created for evaluation of the tungsten and W-25Re for comparative purposes. All deposited microstructures and process parameters are shown in the Appendix of this report for the three materials. Figure 21 in the Appendix shows the micrograph orientation relative to DLF deposit build direction and nomenclature used in this report.

Plasma Spherodized Tungsten Powder--As described previously, studies using plasma spherodized tungsten showed no porosity in DLF deposited rods. Single pass plates, with a thickness equivalent to one molten pool diameter, (Figure 1, left) were deposited. The tungsten single-pass plates had little to no porosity, large grain structure growing epitaxially and some cracking. Figure 7 shows the best DLF tungsten microstructure produced after deposition parameters were optimized to laser power= 500w, velocity= 20ipm, and layer depth= 0.005in. Decreasing the laser power to 190w resulted in large intergranular cracks (Figure 8) in the microstructure. Orbital motion (Figure 9), used to build the plate having the microstructure shown in Figure 8, widens the molten pool size to produce a larger melt volume. Using this mode for deposition had no discernable effect on reducing the porosity or cracking in the DLF tungsten microstructure.

Use of the plasma spherodized powder has produced deposits with minimal porosity, however epitaxial growth with intergranular cracking may be a dominant failure mode for this material. Plasma spherodization appears to remove some of the gas in the sodium and potassium reduced powders that form porosity during solidification . Further work is required to identity these gases but these tungsten deposition tests suggest that refractory metal powders need to be out-gassed by plasma re-melting or other processes prior to DLF deposition. Further parameter development may also lead to methods of retarding grain growth through subsequent deposited layers. Stirring or pulsing the molten pool during the process may provide ways of modifying the resultant microstructure.

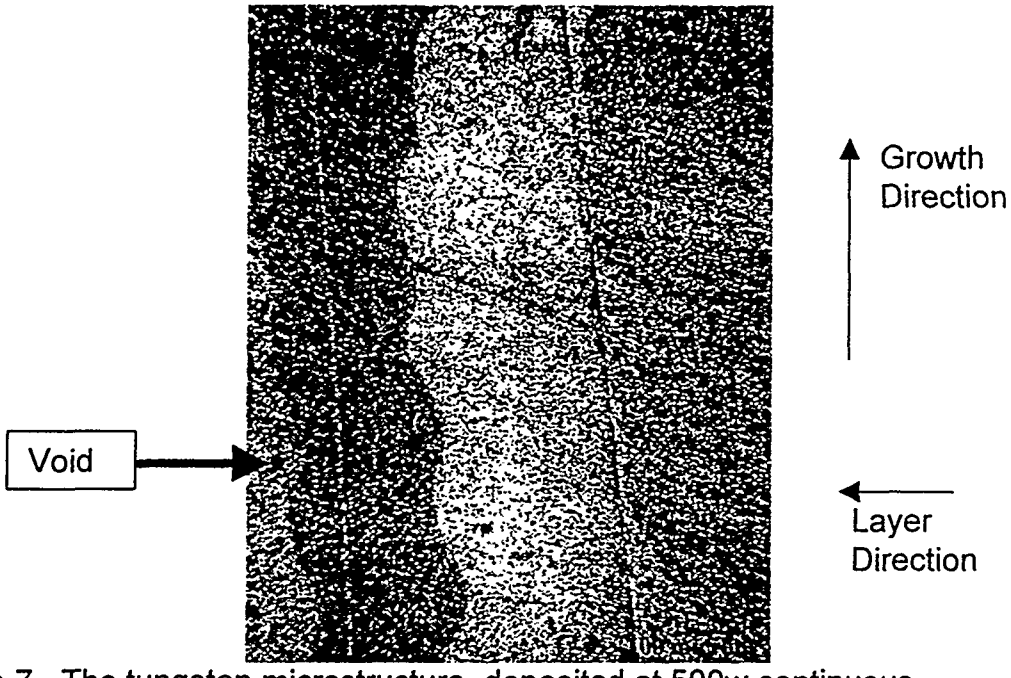

Figure 7. The tungsten microstructure, deposited at 500w continuous wave (CW), layer depth of 0.005" and velocity of 20 inches per minute (IPM). Few voids and no cracks where detected.

Figure 8. This tungsten microstructure, showing a large void and associated crack, was produced with the same parameters as the sample in Figure 7, except the power was lowered to 190w CW.

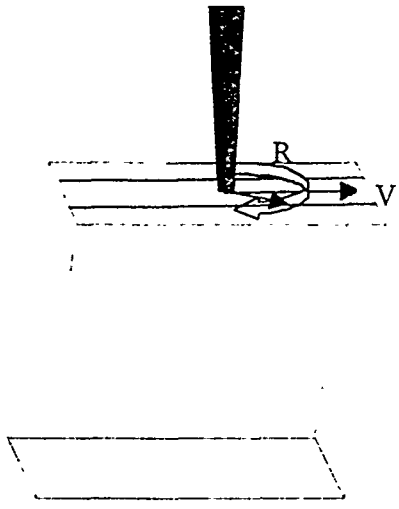

Figure 9. The diagram shows DLF deposition with orbit mode on a multi-pass plate. The orbit mode was used to increase molten pool volume during DLF deposition.

W-25Re Blended Powder—Tungsten and rhenium powders were blended to form a Tungsten-25rhenium alloy composition. The mixture was deposited to form single-pass plates equal in thickness to the molten pool formed. Gas porosity was evident in all of the single-pass plates with pores ranging in approximate size of 10–100μm in diameter. Microstructures of deposits formed at 200w (Figure 10) had a smaller quantity of large pores compared to deposits made at 400w (Figure 11). One possible cause could be that the small molten pool produced at low power cools rapidly, freezing the gas in place before bubbles can form and agglomerate.

The as-deposited microstructure in Figure 10a (40X) shows tungsten particles and gas pores. SEM compositional analysis is shown in Figure 10b (500X). Both two-phase and single-phase regions are visible in the matrix at high magnification. The average composition of the two-phase region was 64W-35Re (atomic %) and the average composition of the single-phase region was 68W-31Re. These compositions are near the pure tungsten-sigma plus tungsten boundary at approximately 70W (atomic %) of the equilibrium phase diagram. The tungsten particles were 97a/oW, indicating that the particles either did not melt or did melt and resolidified quickly enough to minimize dilution into the matrix.

Multi-pass (thick) plates of W-25Re were made after the powder was vacuum baked at 188C for 3.5 days to remove any absorbed gases and water on the powder surfaces. Deposit microstructures had porosity similar to that found in single-pass plates. In addition, increased cracking was evident in the microstructures deposited at 400w (Figure 12) and 590w (Figure 13). Other plates were made by superimposing a square wave pulse on the CW mode, producing a peak power of 250% of CW at a frequency of 500 Hz and a pulse width of 0.7ms. The microstructure in Figure 14 was produced using 400w CW with a square-wave peak power of 1000w. The higher peak power lowered the

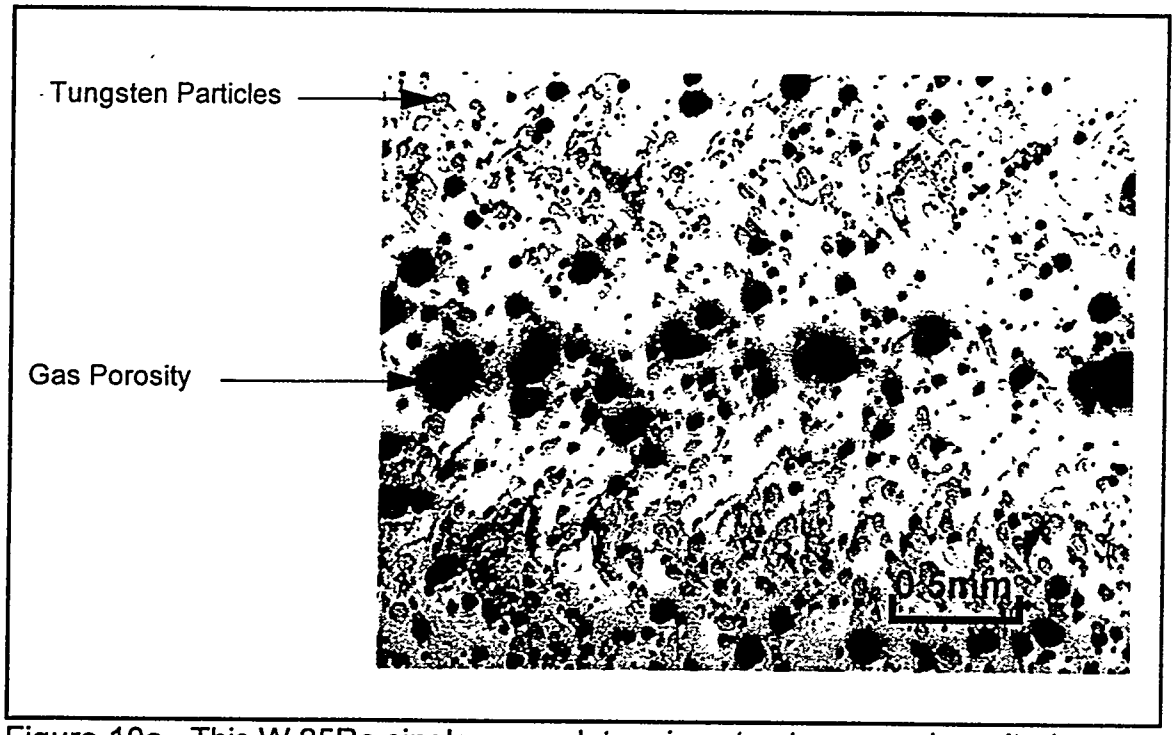

Figure 10a. This W-25Re single pass plate microstructure was deposited at 200w, CW, 5 IPM, and Z-increment of 0.005". Unmelted tungsten particles and gas porosity are evident.

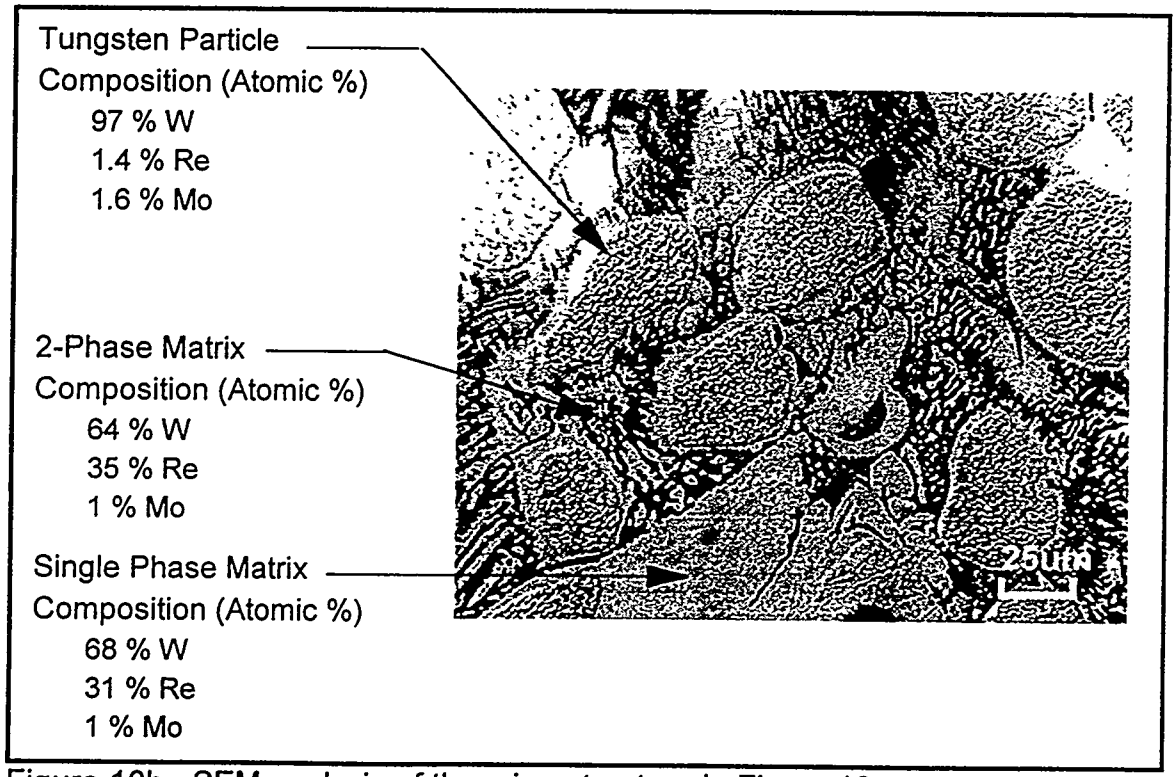

Figure 10b. SEM analysis of the microstructure in Figure 10a.

density of pores and cracks as compared to the CW deposit (Figure 11). The plate microstructure in Figure 15 was produced using orbital motion at 500w CW and no beneficial effect on pore formation was observed.

Additional studies are needed to optimize the W-25Re deposition. The use of a square wave pulse with high peak power appears to warrant further investigation because porosity was reduced with minimal cracking. Available power was limited to less than 590w average power CW because of back-reflection on the fiber delivery optics, however the higher average powers resulted in cracking. The large grain growth with intergranular cracking observed in the pure tungsten studies, was not evident in the W-25Re deposits. Plasma spherodization of the tungsten and rhenium starting powders to try to remove residual gases could reduce the pore formation in the W-25Re as established with the pure tungsten samples that used plasma spherodized powder.

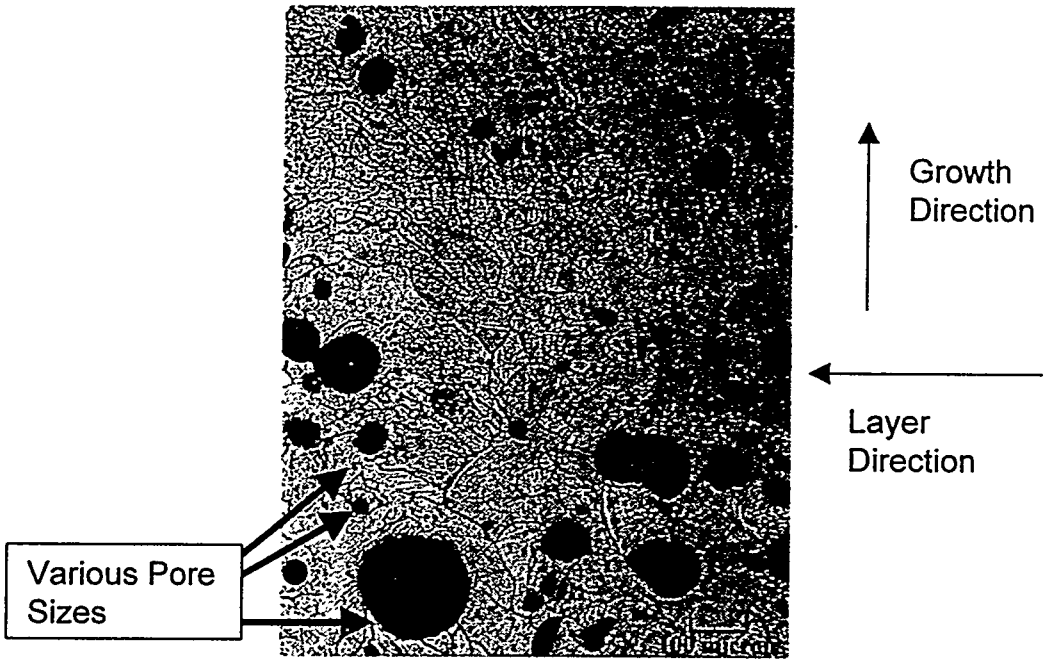

Figure 11. This single-pass plate of a W-25Re microstructure was fabricated at 400w CW at the same parameters as the sample in Figure 10. Larger pores and larger grain structure resulted with complete melting of the powder particles. Spherical pores form from the evolution of entrapped gas in the starting powders.

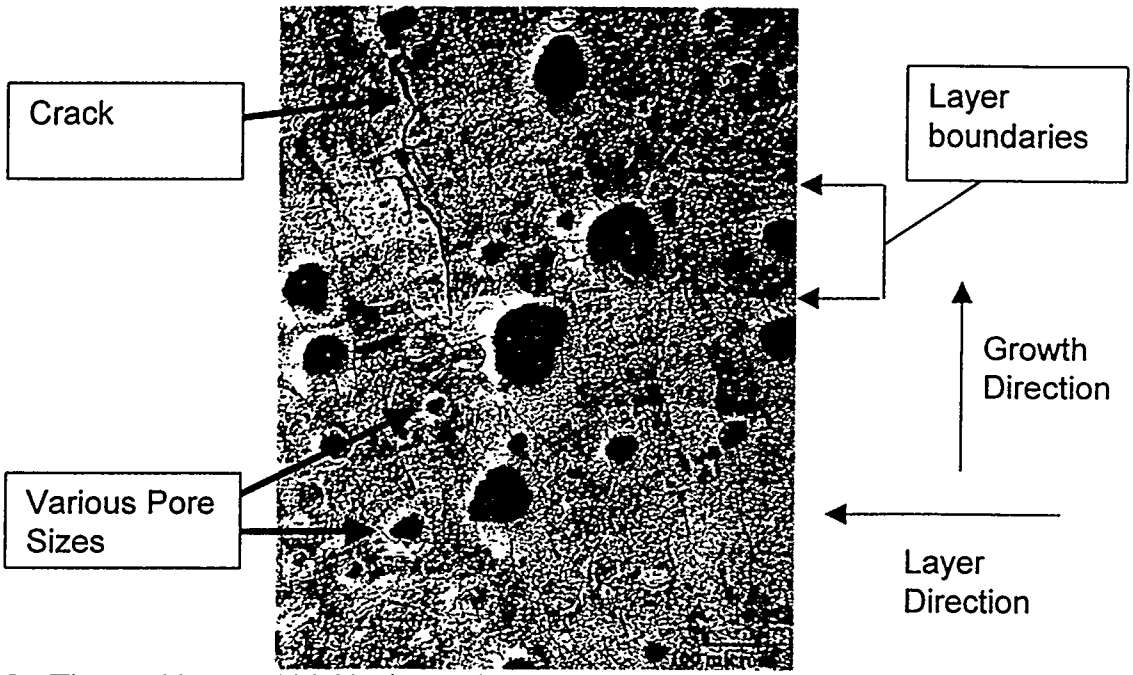

Figure 12. The multi-pass (thick) plate microstructure of W-25Re was produced at 400w CW, velocity of 20 IPM and a Z-increment of 0.0075", showing lower density of pores and cracks as compared to Figure 13 (590w).

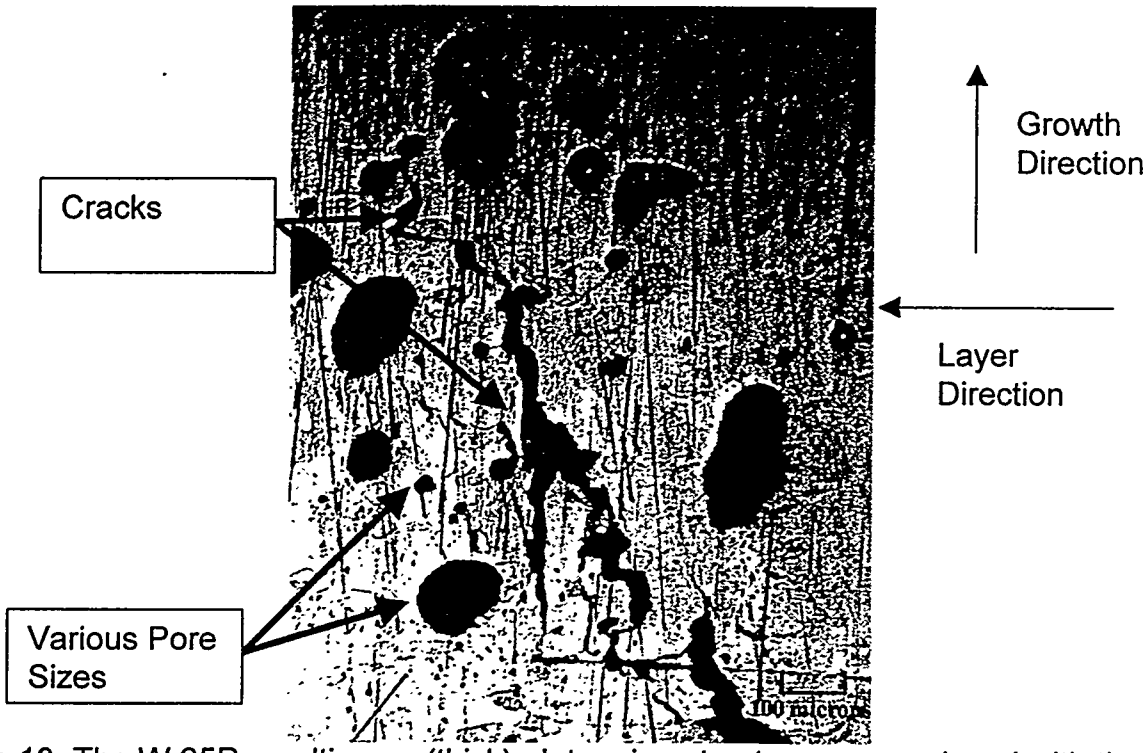

Figure 13. The W-25Re multi-pass (thick) plate microstructure was produced with the same parameters as those for Figure 12, except the power was raised to 590. Pore size and cracks were more predominant, however, all the powder has been melted and resolidified.

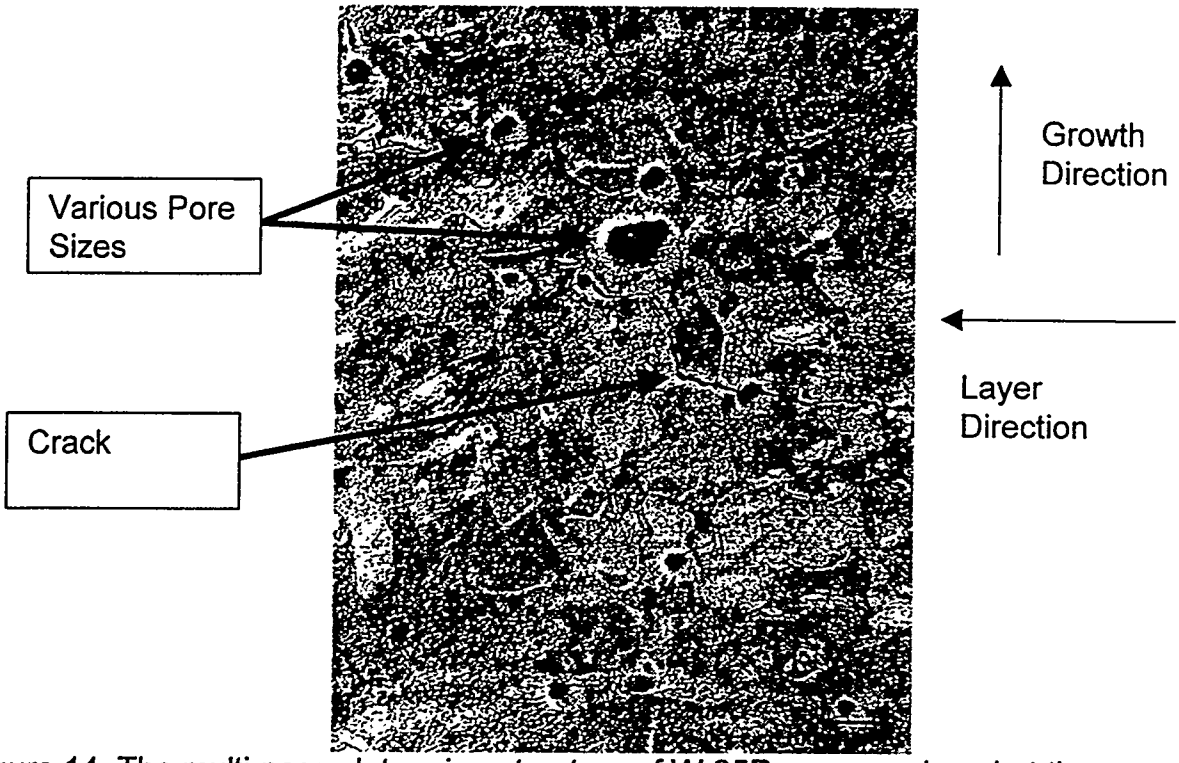

Figure 14. The multi-pass plate microstructure of W-25Re was produced at the same average laser power and parameters as Figure 11, except a square peak pulse was superimposed on the CW power, giving a peak power of 250% over the average power.

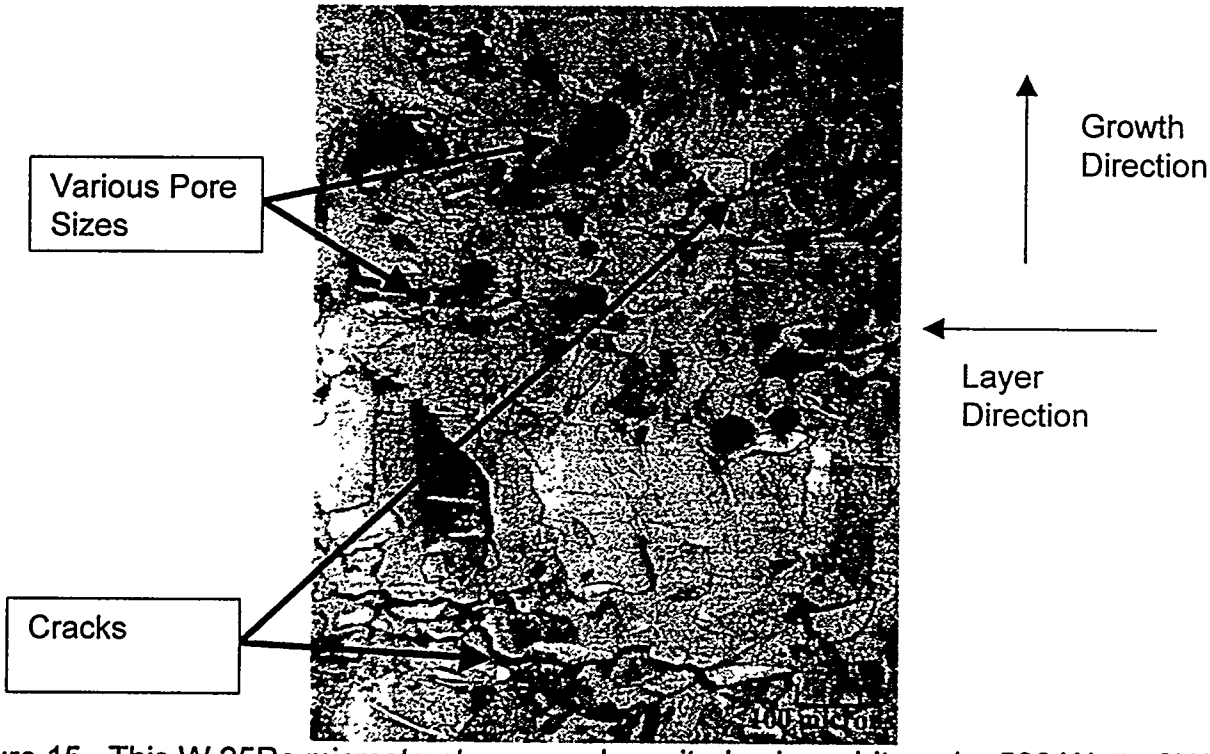

Figure 15. This W-25Re microstructure was deposited using orbit mode, 500 Watts CW, deposition velocity of 20.1 IPM, Z-increment of 0.0075", and powder feed rate of 7.7 g/m.

Niobium Hydride de-hydride powder--Nb multi-pass (thick) plates, made from hydride-dehydride powder (Figure 3), were deposited with minimal cracking and porosity. Epitaxial growth through layer boundaries was evident in the solidification microstructure similar to the pure tungsten deposits. However, epitaxial grains terminating at layer boundaries were common where lack of fusion occurred between layers. For the Nb, velocity, power, and waveform of the laser light were varied to find the optimized parameters to grow fully dense plates. Figures 16 and 17 show that with increase in laser power from 310w to 380w, porosity decreased and better bonding between layers was achieved. By changing the waveform of the laser from CW to a CW plus a superimposed square wave pulse, porosity in the niobium was also decreased (Figure 18). The square wave pulse frequency was 500Hz, pulse width was 0.7 ms, and peak power was 1000w.

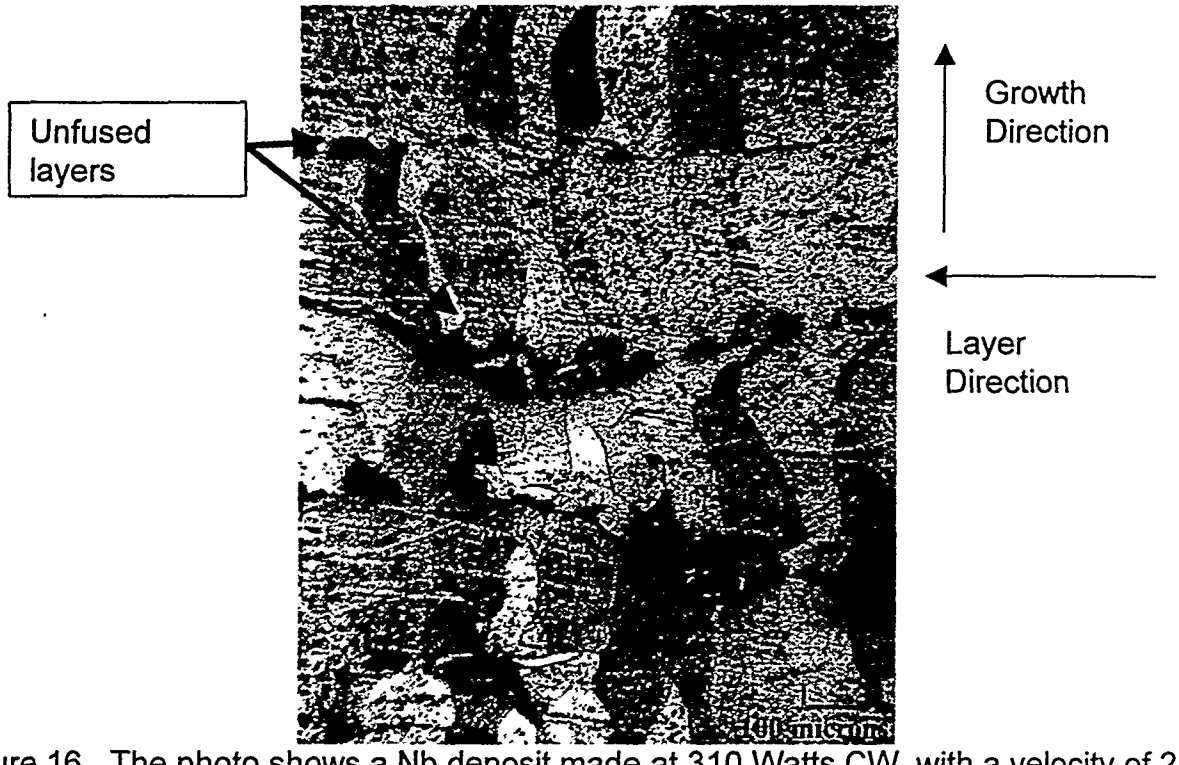

Figure 16. The photo shows a Nb deposit made at 310 Watts CW, with a velocity of 20 IPM, Z-increment of 0.0075", and powder feed rate of 2.4 g/m. Layers are uneven and not fused, however there is no evidence of unmelted powder particles.

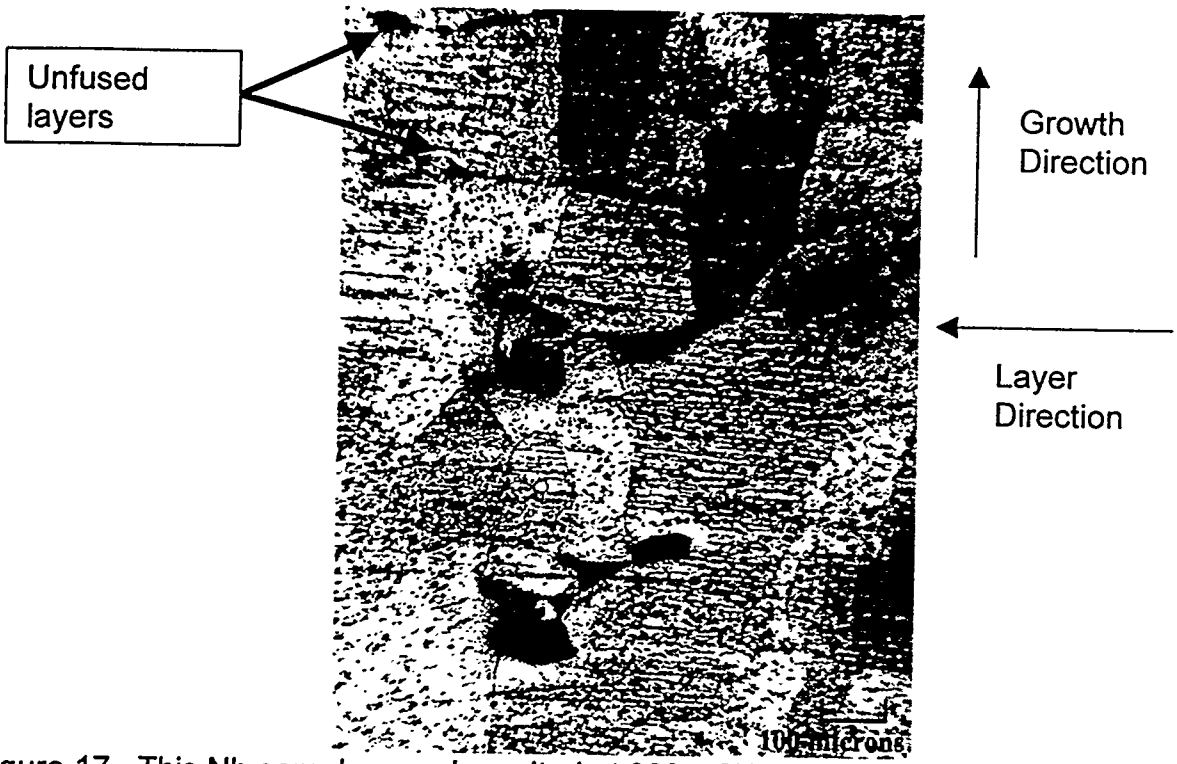

Figure 17. This Nb sample was deposited at 380w CW compared to 310w for the deposit in Figure 16. Lack of fusion across layer boundaries is evident.

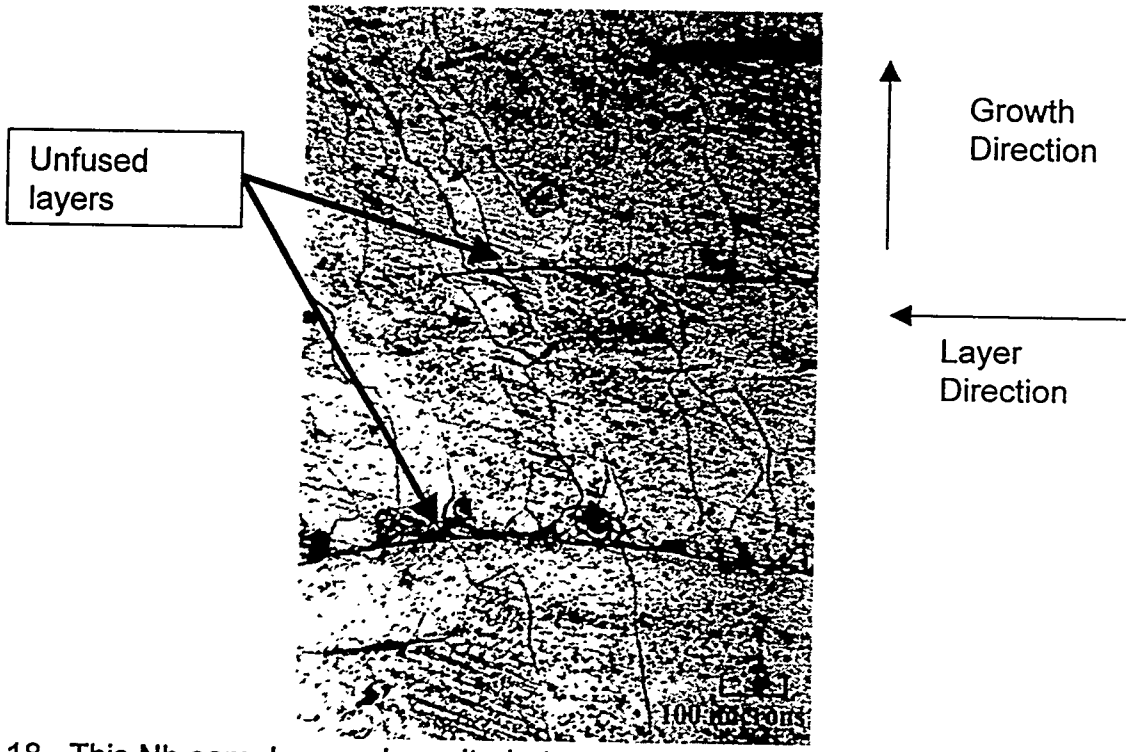

Figure 18. This Nb sample was deposited at an average of 400 Watts with a peak square pulse (1000w) superimposed, without the aid of orbit mode. The feedrate and the Z-increment were identical to Figures 16 (310w) and 17 (380w).

Full density was achieved in the niobium deposits by increasing the power from 400w to 500w with the square wave superimposed (peak power 1250w). Figure 19 shows the microstructure produced at various deposition speeds. The cracks near the top of the photo formed at a velocity 65% greater than previous deposits made at a velocity of 20 IPM. Full density was achieved at 25 IPM (bottom of photo) and could be used for the test bars required for this study, however those were not made at this time because of other difficulties occurring in the processing.

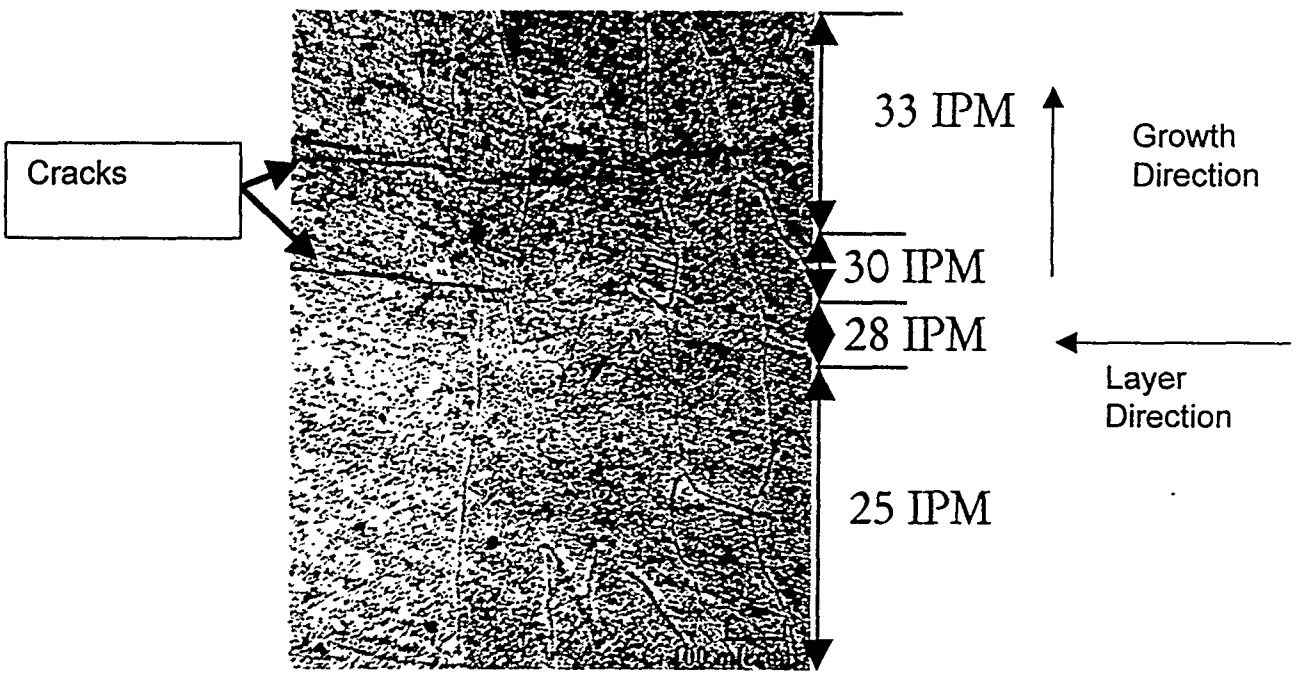

Figure 19. This Nb sample was processed at 500w average power CW with a square peak pulse (1000w) superimposed, giving an increase of 250% the average CW power using orbit motion mode. Velocities range from 23 in. per minute (IPM) at the bottom to 33 IPM, with changes to 25, 28, 30 IPM. The Z-increment of the deposit was 0.0075" and the powder feed rate was 2.4 g/m.

Although samples were produced for parameter optimization and microstructural analysis, attempts to produce full size bars for testing failed because of several problems common to the refractory metals tried so far. Figure 20 shows niobium bars that were started but not finished because of several difficulties. Clogging because of acicular powder particles (see Figure 3) was occurring in the nozzle tip producing non-uniform deposits that inhibited building the niobium bars to the required height. Melting of the aluminum tip of the powder delivery nozzle by the radiant heat from the refractory metal molten pool also caused degradation of the deposit uniformity. The melting tip and powder clogging also produced build-up of material on the nozzle tip, which

interfered with powder delivery. Additionally, available power was limited because of the potential damage to the fiber-optic beam-delivery system by back-reflected laser light from the molten niobium pool. Solid niobium is 78% reflective at the Nd-YAG wavelength of 1.06um (see Table 4) and should be higher in the molten state. These effects produced the non-uniform side structure and irregular globs shown on the three plates attempted.

Table 4. Normal Incidence of Reflection for Various Solid Materials at 1064nm Light, Interpolated from CRC Handbook

Material	Reflection (%)
Cu	98
Fe	62.5
Ir	79.5
Hf	57
Mo	68
Nb	78
Re	68
Ta	88
Ti	55.5
W	60
Zr	13.5

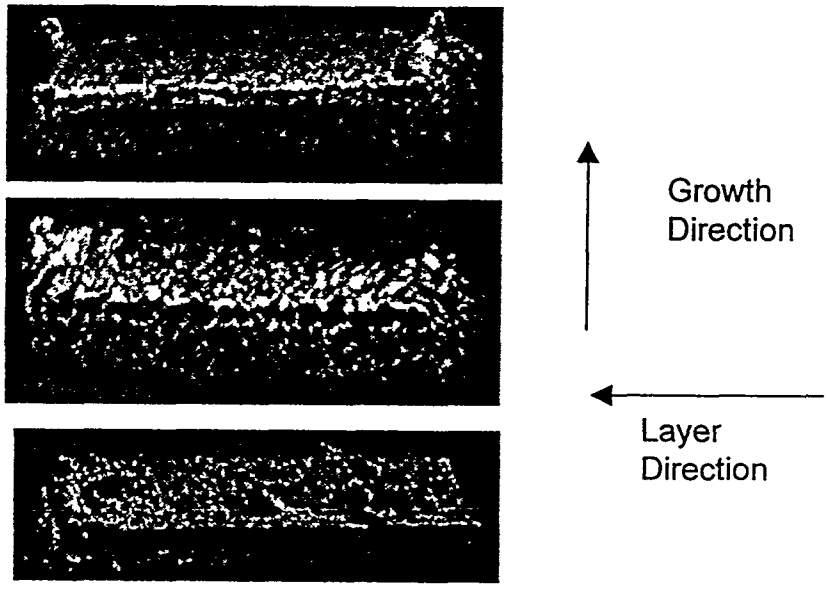

Figure 20. The photograph shows niobium plates deposited at 400w (top), 500w (middle) and 500w (bottom) using orbit mode. Deposition was stopped because of nozzle clogging, nozzle melting, and "glob" formation on the nozzle tip. Reflection of the laser beam back through the beam delivery optics prevented use of powers higher than 500w and limited the parameter range used for this study.

Recommendations

1. From this study, the following optimized DLF processing parameters are recommended for deposition of the required plates.

   A. Spherodized tungsten powder - 500 watts CW, feedrate of 20 IPM, Z-increment of 0.005", Powder feed of 10.1 g/m.
   B. W-25Re - 400 watts average power CW plus 1000w peak power square wave pulse, feedrate of 20 IPM, Z-increment of 0.0075", Powder feed of 7.7 g/m
   C. Nb - 500 Watts Square Wave Pulse, Feedrate of 25 IPM, Z-increment of 0.0075" Powder feed of 2.4 g/m

2. Further, gas analysis of starting powders compared to the DLF deposits are necessary to identify the gases being evolved during deposition.

3. An evaluation of powder processing methods to remelt/spherodize powders for gas reduction in DLF deposits is required to remove the interstitial gases in the starting powders.

4. Powder feed for non-spherical refractory metal powders must be evaluated to prevent nozzle clogging.

5. A higher melting temperature material for the nozzle is required to prevent the nozzle from melting during processing.

6. Potential damage to the beam delivery system by reflections must be prevented by better design, which will allow higher Nd-YAG power to be used and will enhance the processing envelope available for refractory metals and other highly reflective metals.

Acknowledgements

The authors thank Ann Kelly (MST-6) for metallographic work performed on the samples and Julie Bremser (MST-6) for the interstitial gas analysis on the starting powders.

References

1. Lewis, G.K., Milewski, J.M., Nemec, R.B., Thoma, D.J., Cremers, D.A., and Barbe, M.R., October 17-21, 1994, Directed Light Fabrication, International Conference on Lasers and Electro-Optics, (ICALEO '94), Orlando, Florida.

2. J.O. Milewski, G.K. Lewis, P. Dickerson, J.C. Fonseca, R.B. Nemec, "Application of a Manufacturing Model for the Optimization of Additive processing of Inconel Alloy 690", Journal of Materials Processing Technology, November 1997.

3. Lewis, G.K., Thoma, D.J., Milewski, J.O., Nemec, R.B., June 16-21, 1996, Directed Light Fabrication of Near-Net Shape Metal Components, World Congress on Powder Metallurgy and Particulate Materials, Washington, D.C.

4. Weaver, J. H. and Frederikse, H.P.R. "Optical Properties of Metals and Semiconductors" CRC Handbook of Chemistry and Physics. Vol.78, 1997-1998

Appendix--Data

This appendix presents the DLF deposition test parameters for the tungsten, tungsten-25rhenium, and niobium materials studied. Also shown is the associated metallography for all tests conducted in the program.

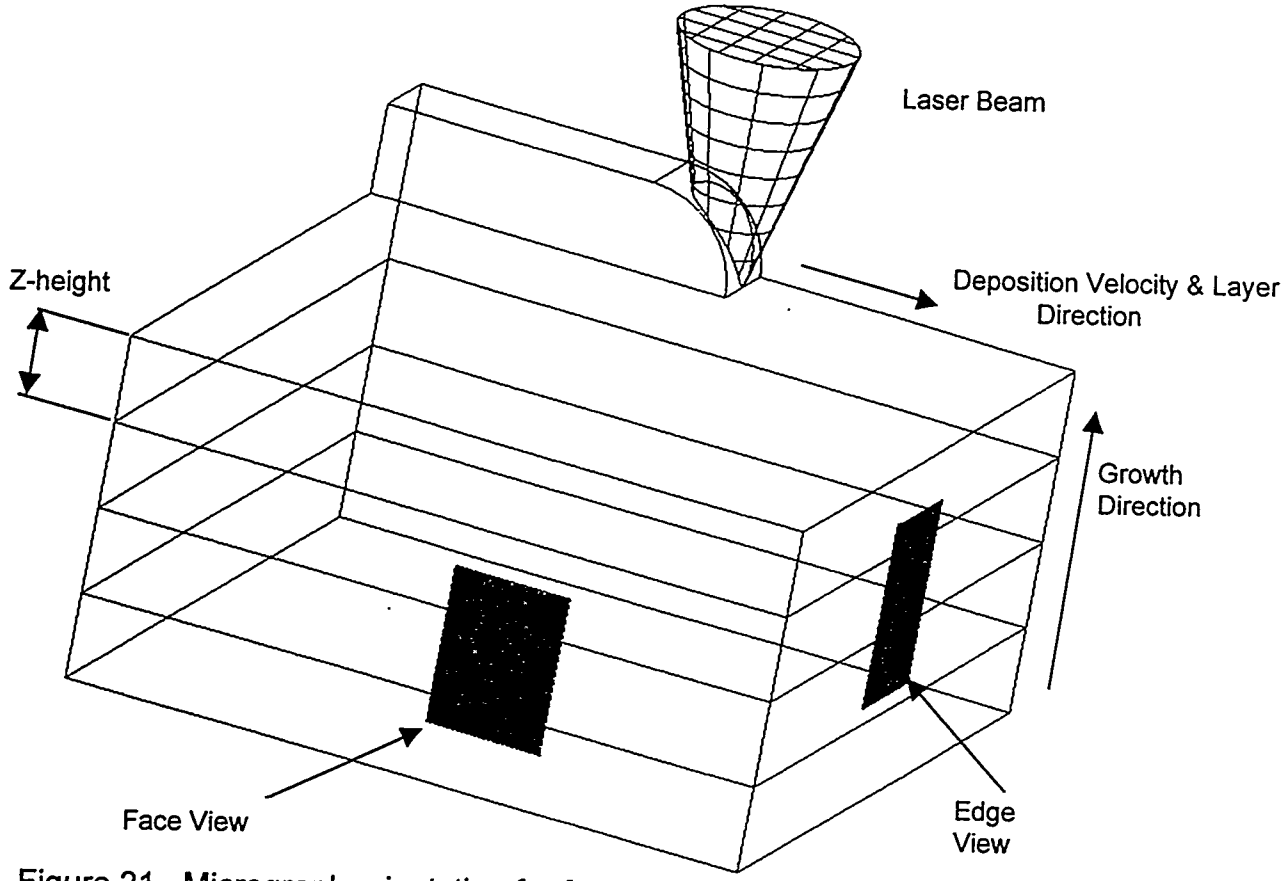

Figure 21. Micrograph orientation for face and edge views relative to DLF deposit.